The $e^+e^- \to \mu^+\mu^-$ Cross Section in the Standard Model

Alex Pearce

April 3, 2012

Abstract

The Standard Model's (SM) prediction of particles beyond those initially considered by quantum electrodynamics (QED) has yielded excellent results. The Super Proton Synchrotron (SPS) at CERN recently detected both the W bosons and the Z boson via the $p\bar{p}$ channel (Rubbia, van der Meer et al.). We performed a numerical integration of the differential cross section of the $e^+e^- \to \mu^+\mu^-$ scattering process, which may produce Z bosons, in the hope that the proposed Large Electron-Positron collider (LEP) will verify this channel of Z production. A distinct Z resonance around the Z mass of 91.8GeV was found with a cross section $\sigma = 9.4\text{nb}^{-1}$.

1 Introduction

The proposition of three mediators of the weak nuclear force, the W^+, W^- and Z bosons, has been all but proven by the current team at CERN operating the SPS. The suggestion of Z production via electron-positron pairs is now becoming of interest to experimentalists. The process is manifested by an electron-position pair (e^-e^+) annihilating, forming either a virtual photon or Z boson, and then a muon-antimuon pair ($\mu^-\mu^+$) being produced.

This interaction is described by the Feynman diagram in figure 1a. The scattering is also described by a t-channel diagram (in figure 1b), however we proceed by analysing the s-channel as it is only this channel via which we may measure resonances and new unstable particles. Note that a u-channel diagram also exists, but as it is simply a swapping of the outgoing particles' momenta in the t-channel, hence we ignore this also.

The use of Feynman diagrams is that we may apply the Feynman rules to them to produce a matrix element $\mathcal{M}$. The square of this corresponds to a differential cross section $\frac{\mathrm{d}\sigma}{\mathrm{d}\Omega}$ which may be integrated to find the total cross section σ, which is measurable by a detector.

The following section briefly outlines the theory behind the interactions. The integration methods used to evaluate the differential cross sections are explored in the section after that, along with a study of the differential cross sections in order to judge the effectiveness of numerical integration upon them. The results

are presented and analysed in section 4, then a discussion of the kinematic variables follows in section 5. Finally, a brief discussion on performance and alternative numerical integration techniques occurs in section 6.

2 Principles of Interaction Cross Sections

With reference to the Feynman diagrams in figures 1a and 1b, the incoming particles are labelled with the four-momenta p_1^ν and p_2^ν, whilst the outgoing particles carry p_3^ν and p_4^ν. At LEP, the electrons and positrons (antiparticles to the electron) will be accelerated around a loop in opposite directions. The collider energy is then given $\sqrt{s}$, where

$$s = (p_1 + p_2)^2.$$

Here we have suppressed the metric tensor and covariant notation, implicitly assuming four vectors. The collider energy is then analogous to the hypotenuse of a right-angled triangle of sides p_1^ν and p_2^ν.

The differential cross sections are dependant on the collider energy via the dimensionless variables

$$\varepsilon = \frac{m_\mu}{\sqrt{s}}, \quad \lambda = \frac{M_Z}{\sqrt{s}},$$

where m_μ is the muon mass. It is worth noting that, at the energies LEP will be operating at, it is safe to consider the electron as massless in the ultra-relativistic limit. (In addition, the muon is over 200 times more massive than the electron so we may disregard the electron mass in scattering interactions.)

2.1 Real and Virtual Particles

As noted in figure 1a, the scattering may be mediated by either a virtual photon γ^* or a $Z^{(*)}$ boson, where the bracketed star notation indicates that the boson may either be *on-* or *off-mass-shell*. These terms refer to how well the mediating particles (propagators in the Feynman diagrams) adhere to the mass-energy relation $E^2 - |\vec{p}|^2c^2 = m^2c^4$. Propagators exceeding the classical relativistic values of E and p are off-shell, and said to be virtual particles. This violation of relativity is allowed because it is permitted by the Heisenberg uncertainty principle, $\Delta E \Delta t \geq \hbar$: the violation in energy may only exist for a very small amount of time.

The Z boson will be on-shell (i.e. real) if and only if $s = M_Z$, where M_Z is the boson's mass. When the particle is real, we can detect it. With this, we should expect a cross section resonance as the boson tends towards being on-mass.

2.2 Differential Cross Sections

The total matrix element $\mathcal{M}$ must be considered carefully. As the propagator in the interaction may be one of two particles, it must be the sum of two

separate matrix elements (one matrix element for each possible propagator). The measurable quantity, the cross section, is the integrated square of the matrix element, so we must have the square of a sum:

$$\begin{aligned}
\mathcal{M} &= \mathcal{M}_\gamma + \mathcal{M}_Z, \\
\mathcal{M}^2 &= (\mathcal{M}_\gamma + \mathcal{M}_Z)^2 \\
&= \mathcal{M}_\gamma^2 + \mathcal{M}_Z^2 + 2\,\mathrm{Re}(\mathcal{M}_\gamma \mathcal{M}_Z^*) \\
&= \frac{\mathrm{d}\sigma}{\mathrm{d}\Omega}^{\gamma\text{-}\gamma} + \frac{\mathrm{d}\sigma}{\mathrm{d}\Omega}^{Z\text{-}Z} + \frac{\mathrm{d}\sigma}{\mathrm{d}\Omega}^{\gamma\text{-}Z} \\
&= \frac{\mathrm{d}\sigma}{\mathrm{d}\Omega}.
\end{aligned}$$

Each term of $\mathcal{M}^2$ corresponds to its own differential cross section: the first for the pure photon process, the second for the pure Z process, and the last for the interference of both processes.

The functional form of each differential cross section is derived by applying the Feynman rules to figure 1a. Due to their bulk, they are not reproduced here but are given in appendix A.

3 Integration of the Differential $\frac{\mathrm{d}\sigma}{\mathrm{d}\Omega}$

A common analytical approach to numerically approximating integrals in the trapezium rule. We use the trapezium rule and compare it with the much more recent Monte Carlo method, whereby random points are sampled and the fraction of those between the curve and the independent axis is proportional to the area i.e. the integral.

The reasoning behind using two methods of numerical integration is twofold. Firstly, it serves as a useful consistency check: if at least one method is running incorrectly, the results from each are unlikely to agree with each other. Secondly, the data collected with respect to the efficiency of each method on the given functions may be useful for future analysis of particle interaction cross sections (or, indeed, any functions of a similar form).

On this point, it is worth noting that the accuracy of each algorithm will depend largely on the functional form of the differential cross sections. Erratic, non-analytic functions will be poorly suited for trapezium evaluation, while functions with very small variations will result in the poor Monte Carlo accuracy. The differential forms are plotted in figures 2, 3 and **??**. The impact of these forms in the accuracy of the final results will be analysed in section 4.

3.1 Method

Firstly, we observe that they is no ϕ dependence in any of the differential cross sections. This makes the integration over ϕ trivial ($0 \leq \phi \leq 2\pi$), adding a factor

of 2π to cross section σ. This simplifies the problem significantly as we are now dealing with a one-dimensional integral and so may use the trapezium rule.

As the integration is over circular polar coordinates, we note that the differential $\sin\theta \, \mathrm{d}\theta \, \mathrm{d}\phi$ may be expressed as $\mathrm{d}(\cos\theta) \, \mathrm{d}\phi$, hence we may perform the change of variable $\cos\theta \to x$. This changes the limits in θ to the limits in x

$$0 \leq \theta \leq \pi \to -1 \leq x \leq 1.$$

Consequently, the random numbers generated for the Monte Carlo integration are generated between -1 and 1, providing a uniform distribution in $\cos\theta$, rather than θ.

A simple Monte Carlo integration will be performed via

$$\int_a^b f(x) \, \mathrm{d}x \approx \frac{b-a}{N} \sum_{i=1}^{N} f(x_i),$$

where N is the number of random points to be sampled and x_i is the i^{th} random number within the limits of integration.

A similarly simple trapezium algorithm is used:

$$\int_a^b f(x) \, \mathrm{d}x \approx \frac{h(f(a)+f(b))}{2} + h \sum_{i=1}^{N-1} f(a+ih), \quad h = \frac{b-a}{N}.$$

h is the trapezium width and N is the number of trapezoids used to estimate the integral with.

Both methods are quoted as approximations, but it should be considered that as $N \to \infty$ the Monte Carlo method becomes exact (despite this being impossible to perform computationally).

The number of points to sample or the number of trapezoids to use will depend on the computation power and time available, as well as the accuracy and precision desired. The exact values used will be discussed in the following section.

4 Results and Analysis

TODO: discuss step size, errors, and iterations.

The integrated cross section is presented in figures 4a and 4b. Each plot shows both the trapezium and Monte Carlo integration results, but their correspondence is such that they are almost indistinguishable from one another.

The Monte Carlo cross section shows slight fluctuations on a scale of 10^{-8} GeV^{-2} but is clearly following the trapezium curve precisely.

There is a striking Z resonance around the Z mass M_Z. The cross section peaks to 8.17×10^{-7} GeV^{-2} at collider energy 91.21 GeV. It is important to note that this is *above* the Z mass of 91.19 GeV. The explanation for this cannot be

the γ - γ channel as there is clearly no resonance is its cross section (figure 4a). It is due to the Standard Model contribution, and in particular the interference term γ - Z.

Figure 6 shows the cross section for the interference term as evaluated by the Monte Carlo method, with the trapezium algorithm superimposed (figure 6a shows just the trapezium algorithm's evaluation).

5 Kinematic Variables

Discussion of $\cos\theta$ and $p_T = |\vec{p}_f| \sin\theta$.

6 Performance

TODO Extension of the problem.

6.1 Runge-Kutta

Here we are.

7 Figures

7.1 Feynman Diagrams

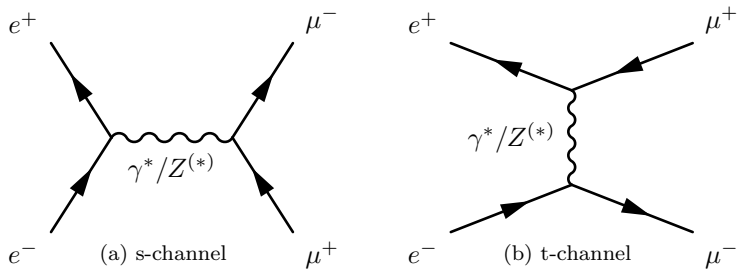

Figure 1: $e^-e^+ \to \mu^-\mu^+$ scattering via two different channels. Time flows from left to right.

7.2 Differential Cross Sections

This subsection contains plottings of the QED differential cross section (γ - γ channel) and then the full Standard Model cross section (γ - γ, Z - Z and γ - Z channels) at three different collider energies.

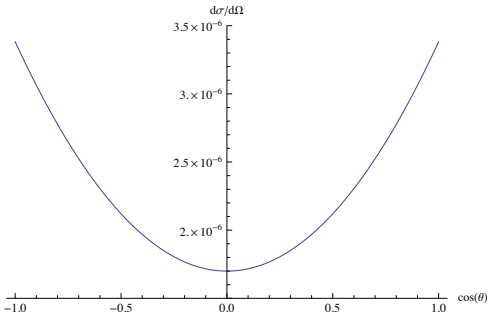

(a) QED

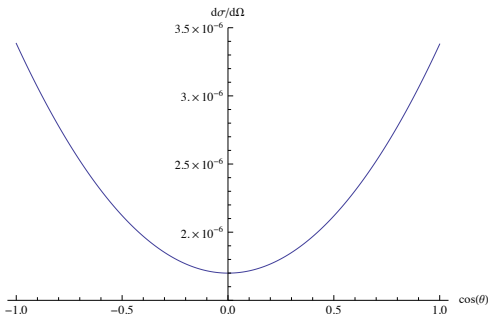

(b) SM

Figure 2: $\frac{\mathrm{d}\sigma}{\mathrm{d}\Omega}$ at $\sqrt{s} = 3$ GeV.

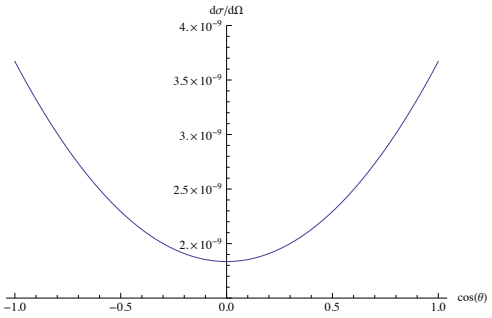

(a) QED

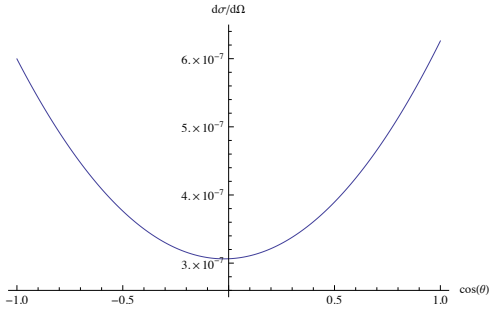

(b) SM

Figure 3: $\frac{\mathrm{d}\sigma}{\mathrm{d}\Omega}$ at $\sqrt{s} = M_Z = 91.2$ GeV.

7.3 Cross Sections σ

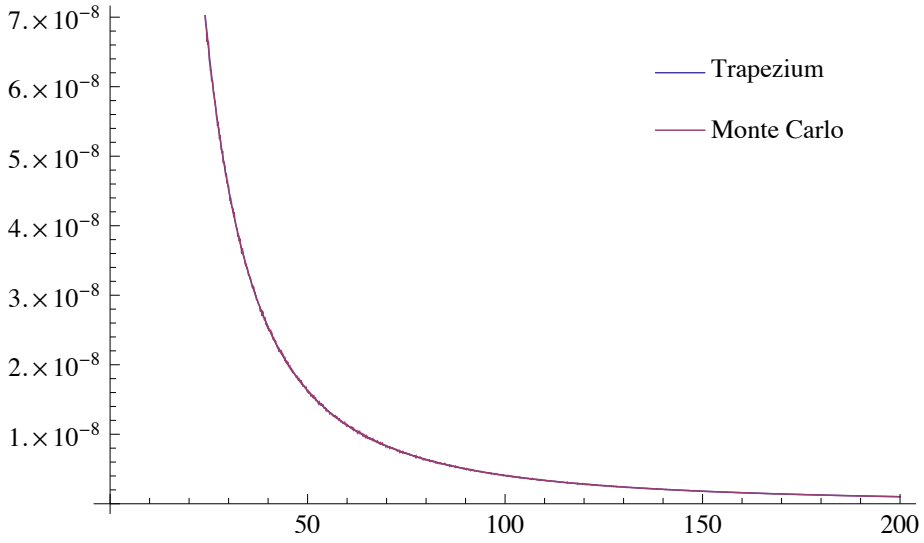

(a) QED

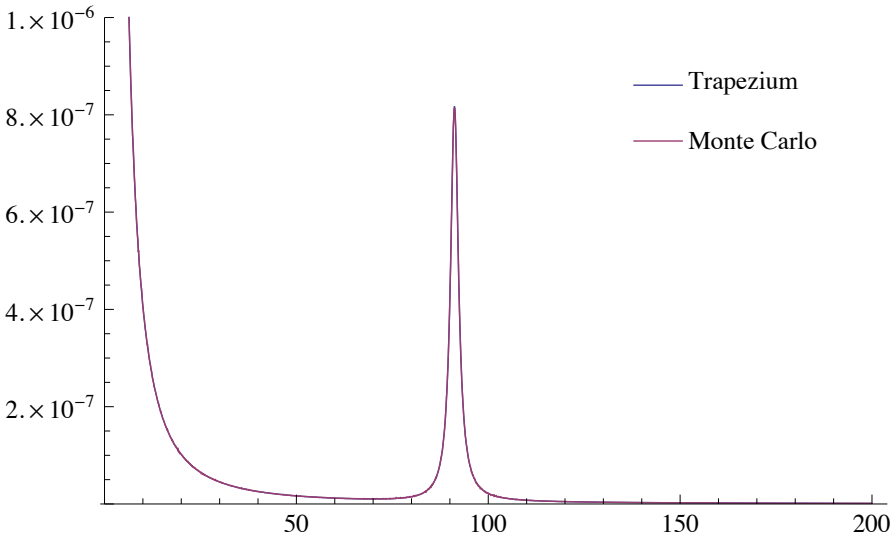

(b) SM

Figure 4: Trapezium and Montecarlo cross section σ for collider energies 3 - 200 GeV.

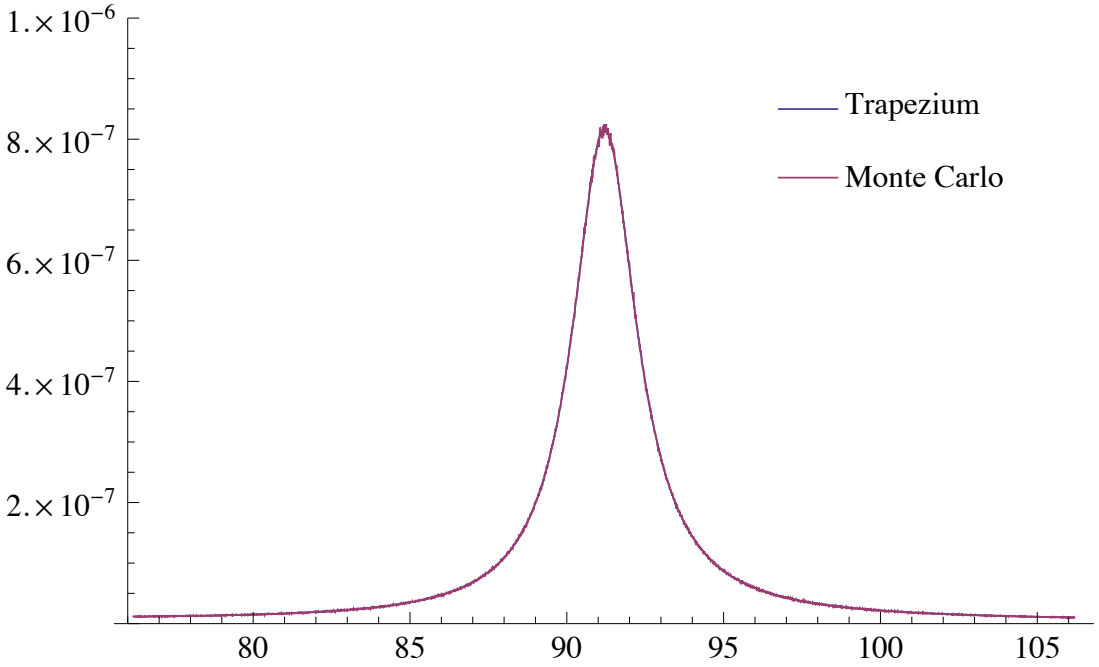

Figure 5: Trapezium and Montecarlo cross section σ for collider energies centred 15 GeV around M_Z.

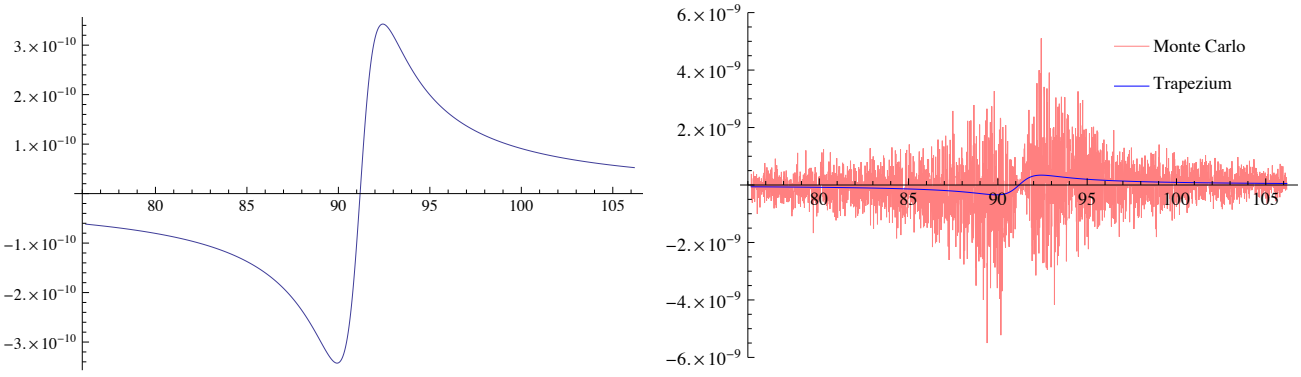

(a) Trapezium

(b) Monte Carlo with trapezium superimposed

Figure 6: γ - Z cross section for collider energies centred 15 GeV around M_Z.

A Differential Cross Sections

The cross sections corresponding to the photon, Z and interference matrix elements follow. Due to the length of the analytic solutions, constants are defined, then the cross section is defined with respect to these constants.

The small energy scales that will be reachable at LEP allow us to take the couplings g_e and g_z as constant. We define $g_e = \sqrt{4\pi\alpha}$ and $g_z = \sqrt{4\pi\alpha}(\cos\theta_w \sin\theta_w)^{-1}$.[1]

A.1 γ - γ

Define

$$\alpha = \frac{g_e^4}{(8\pi)^2 s}\sqrt{1-4\varepsilon^2}.$$

Then

$$\frac{\mathrm{d}\sigma}{\mathrm{d}\Omega}^{\gamma\text{-}\gamma} = \alpha(1+\cos^2\vartheta + 4\varepsilon^2\sin^2\vartheta),$$
$$\sigma^{\gamma\text{-}\gamma} = \frac{16\pi\alpha}{3}(1+2\varepsilon^2). \tag{1}$$

A.2 Z - Z

Define

$$\alpha = \frac{g_Z^4}{(32\pi)^2 s}\frac{\sqrt{1-4\varepsilon^2}}{(1-\lambda^2)^2 + (\frac{\lambda\Gamma_Z}{\sqrt{s}})},$$
$$\beta = ((C_V^e)^2 + (C_A^e)^2)((C_V^\mu)^2),$$
$$\Gamma = ((C_V^e)^2 + (C_A^e)^2)((C_A^\mu)^2)(1-4\varepsilon^2),$$
$$\Delta = 8C_V^e C_A^e C_V^\mu C_A^\mu\sqrt{1-4\varepsilon^2}.$$

Then

$$\frac{\mathrm{d}\sigma}{\mathrm{d}\Omega}^{Z-Z} = \alpha(\beta(1+\cos^2\vartheta + 4\varepsilon^2\sin^2\vartheta) + \Delta(1+\cos^2\vartheta) + \Gamma\cos\vartheta),$$
$$\sigma^{\gamma\text{-}\gamma} = \frac{16\pi\alpha}{3}(\Gamma + (1+2\varepsilon^2)\beta). \tag{2}$$

[1] α is taken to be $\frac{1}{128}$, $\sin^2\theta_w$ is taken to be 0.23152.

A.3 γ - Z

Define

$$\begin{aligned}
\alpha &= \frac{g_Z^4}{(32\pi)^2 s}\frac{\sqrt{1-4\varepsilon^2}}{(1-\lambda^2)^2+(\frac{\lambda\Gamma_Z}{\sqrt{s}})},\\
\beta &= ((C_V^e)^2+(C_A^e)^2)((C_V^\mu)^2),\\
\Gamma &= ((C_V^e)^2+(C_A^e)^2)((C_A^\mu)^2)(1-4\varepsilon^2),\\
\Delta &= 8C_V^eC_A^eC_V^\mu C_A^\mu\sqrt{1-4\varepsilon^2}.
\end{aligned}$$

Then

$$\begin{aligned}
\frac{\mathrm{d}\sigma}{\mathrm{d}\Omega}^{\gamma-Z} &= \alpha(\beta(1+\cos^2\vartheta+4\varepsilon^2\sin^2\vartheta)+\Delta\cos\vartheta),\\
\sigma^{\gamma-Z} &= \frac{16\pi\alpha\beta}{3}(1+2\varepsilon^2). \qquad (3)
\end{aligned}$$

References